

Acceleration of uranium beam to record power of 10.4 kW and observation of new isotopes at Facility for Rare Isotope Beams

P. N. Ostroumov^{1,2}, O. B. Tarasov,¹ N. Bultman,¹ F. Casagrande,¹ Y. Choi,¹ S. Cogan,¹ M. Cortesi,¹ K. Fukushima,¹ A. Gonzalez,^{1,2} J. Guo,¹ K. Haak,^{1,2} M. Hausmann,¹ K. Hwang,¹ M. Ikegami,¹ D. Kaloyanov,^{1,2} T. Kanemura,¹ S.-H. Kim,¹ E. Kwan,¹ M. Larmann,¹ S. Lidia,¹ G. Machicoane,¹ T. Maruta,¹ S. Miller,¹ Y. Momozaki,^{1,3} D. Morris,¹ A. Plastun,¹ M. Portillo,¹ X. Rao,¹ I. Richardson,^{1,2} B. M. Sherrill,^{1,2} M. K. Smith,¹ J. Song,¹ M. Steiner,¹ A. Stolz,^{1,2} S. Watters,^{1,2} J. Wei,^{1,2} T. Xu,^{1,2} T. Zhang,¹ Q. Zhao,¹ S. Zhao,¹ D. S. Ahn,⁴ J. Hwang,⁴ T. Sumikama,⁵ and H. Suzuki⁵

¹Facility for Rare Isotope Beams, Michigan State University, East Lansing, Michigan 48824, USA

²Department of Physics and Astronomy, Michigan State University, East Lansing, Michigan 48824, USA

³Nuclear Science and Engineering Division, Argonne National Laboratory, Lemont, Illinois 60439, USA

⁴Center for Exotic Nuclear Studies, Institute for Basic Science, Daejeon 34126, Republic of Korea

⁵RIKEN Nishina Center for Accelerator-Based Science, RIKEN,

2-1 Hirosawa, Wako, Saitama 351-0198, Japan



(Received 12 February 2024; accepted 31 May 2024; published 17 June 2024)

The Facility for Rare Isotope Beams (FRIB) is a major nuclear physics facility for research with fast, stopped, and reaccelerated beams that was successfully commissioned in May 2022. A key capability of FRIB is the production of an acceleration of the uranium beam, but this capability requires the facility to work at the design limits of the lowest charge-to-mass ratio and the highest power density on the beam intercepting devices. This paper presents techniques for overcoming the significant challenges in accelerating the uranium beam, culminating in the demonstration of 10.4 kW on target, and the discovery of three new isotopes. The high-power uranium beam enabled us to produce and identify ⁸⁸Ga, ⁹³As, and ⁹⁶Se, within the first 24 h of operation. The successful uranium operation at FRIB sets a new record for accelerated uranium beam power above 10 kW and opens a new avenue of research with rare isotopes.

DOI: [10.1103/PhysRevAccelBeams.27.060101](https://doi.org/10.1103/PhysRevAccelBeams.27.060101)

I. INTRODUCTION

The Facility for Rare Isotope Beams, FRIB, [1,2] is the culmination of state-of-the-art advancements in accelerator physics and technology, such as superconducting electron cyclotron resonance (ECR) ion source technology, heavy-ion radio frequency quadrupole (RFQ) technology, large-scale cryogenic and superconducting radiofrequency resonator systems, a large acceptance fragment separator including fragmentation target and beam dump and heavy ion stripping with a thin liquid lithium film, simultaneous acceleration of multiple-charge-state heavy ion beams. The layout of the FRIB linac is shown in Fig. 1. The main features of the FRIB driver linac were described in multiple publications; see, for example, Refs. [3,4]. The recent status of the accelerator and plans for the beam power ramp-up were reported in Ref. [5]. One of the key capabilities of

FRIB is the ability to produce and accelerate beams of the most stable elements. Uranium stands out as the most difficult and important element to accelerate. Of the 17 highest-priority scientific programs with rare isotope beams identified by the National Academy of Science [6] and the Nuclear Science Advisory Committee [7], more than half require a uranium primary beam that can produce an abundant variety of isotopes after fragmentation on a thin target. Therefore, establishing the acceleration of a uranium beam with unprecedented power on the fragmentation target is a crucial milestone for the facility. A uranium beam has been the focus of other rare isotope beam facilities, such as the Radioactive Isotope Beam Factory at RIKEN in Japan [8]. Following 13 years of operation, RIKEN has achieved 9.6 kW of uranium beam power on target, with 5.8 kW offered for users [9]. In this paper, we report that FRIB achieved 10.4 kW of uranium beam power on target in the second year of operation. We further report that it was done on the first attempt. This achievement was made possible by the advantages provided by a continuous-wave (cw) linear accelerator.

This paper consists of five sections describing (i) the production of highly charged uranium ions and beam

Published by the American Physical Society under the terms of the *Creative Commons Attribution 4.0 International* license. Further distribution of this work must maintain attribution to the author(s) and the published article's title, journal citation, and DOI.

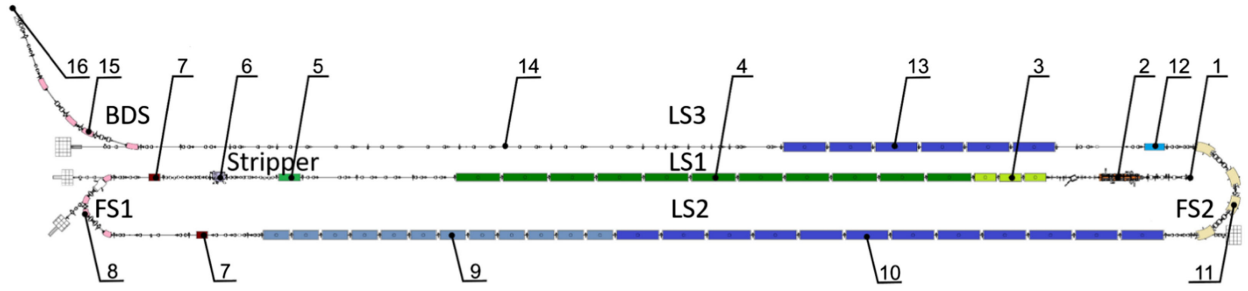


FIG. 1. Layout (top view) of the FRIB accelerator in the tunnel (the above-grade portion of the front end is not shown). 1, 10-m vertical drop from ion sources (above ground); 2, 0.5 MeV/u RFQ; 3, three $\beta = 0.041$ quarter-wave resonator (QWR) cryomodules; 4, 11 $\beta = 0.085$ QWR cryomodules; 5, $\beta = 0.085$ QWR cryomodule; 6, lithium stripper; 7, multigap buncher; 8, room temperature folding segment; 9, 12 $\beta = 0.29$ half-wave Resonator (HWR) cryomodules; 10, 12 $\beta = 0.53$ HWR cryomodules; 11, superconducting folding segment; 12, $\beta = 0.53$ bunching cryomodule; 13, six $\beta = 0.53$ HWR cryomodules; 14, beam transport to the target; 15, beam delivery system (BDS); 16, fragmentation target. Linac segment 1 (LS1): 3–5; folding segment 1 (FS1): 7–8; Linac segment 2 (LS2): 9–10; folding segment 2 (FS2): 11; linac segment 3 (LS2): 12–14; beam delivery system (BDS): 15.

tuning in the front end (FE), (ii) linac tuning methodology, (iii) charge stripping with liquid lithium film, (iv) novel techniques for tuning three charge states of uranium simultaneously and minimizing uncontrolled beam losses, and (v) experimental results identifying new isotopes.

II. PRODUCTION AND TUNING OF URANIUM BEAM IN THE FRONT END

Uranium ions were produced in the FRIB high-performance ECR ion source, which was developed in collaboration with Lawrence Berkeley National Laboratory [10]. The ECR operated at 18 GHz, and the uranium extracted from the plasma chamber biased at 18 kV. The oven and sputtering methods were tested for the production of uranium ions. Although high intensity with up to 60 μA of U^{35+} was produced with the oven method, the beam stability was not as good as the sputtering method, and frequent oven adjustments were necessary. In the sputtering method, neutral uranium vapor is created inside the chamber using an oxygen-dominated ECR plasma to sputter material from a uranium sample biased negatively. A maximum of 33 μA was obtained for U^{35+} when coupling up to 1.5 kW microwave power in the ion source and applying -1.8 kV on the sputter sample. Beyond -1.8 kV on the sputter sample, the intensity extracted was relatively insensitive to the sputter voltage. The 18 GHz Klystron limited the microwave power, and we expect higher performance if more microwave power were available. A typical charge state distribution (CSD) of the uranium ion beam during the ramping up of the beam intensity is shown in Fig. 2, and it is centered between the uranium charge state $34+$ and $35+$. At low intensity, the CSD shows only a small amount of contaminant outside of uranium and oxygen, namely nitrogen and carbon. Uranium charge states up to U^{41+} are visible on the CSD. Uranium beam production from the ion source was sustained over 80 h with excellent beam current stability and was

produced with minimum adjustments of any of the ECR plasma parameters. For most beam operations, ion source pressure remained low at 10^{-8} Torr.

The beam tuning in the low energy beam transport (LEBT) starts with the emittance measurements of the selected charge state $^{238}\text{U}^{35+}$. The 32-m long LEBT contains two 90° combined-function bending magnets, 22 electrostatic quadrupoles, two 90° electrostatic deflectors, and 9 solenoids [11]. The optical simulations were performed with the beam envelope code FLAME [12] using the results of emittance measurements. Two 20-mm aperture collimators located 1.1 m apart to allow phase advance of the transverse oscillations $\sim 60^\circ$ are used to eliminate beam halo in the phase space. These collimators remove $\sim 5\%$ of the total beam intensity, resulting in a reduced beam halo, and create a more compact beam phase space. The beam profile measurements in the medium energy beam transport show the effectiveness of the collimation. The beam central trajectory was tuned using the Bayesian optimization technique [13] to achieve the

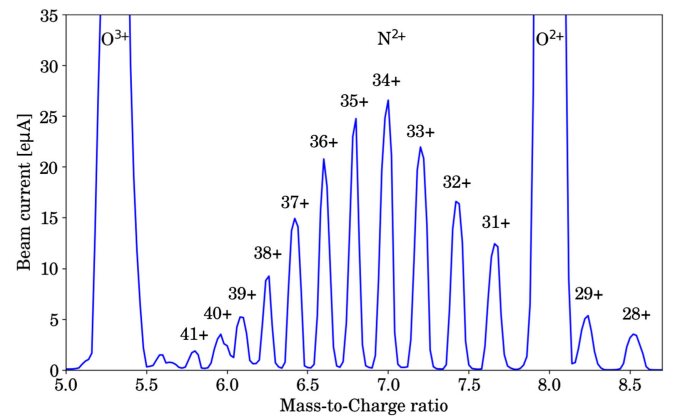


FIG. 2. Charge state distribution for the uranium beam extracted from the high performance electron cyclotron resonance (HP-ECR) ion source.

highest transmission of 70% through the LEBT and RFQ in the presence of the beam collimation.

III. LINAC TUNING METHODOLOGY

The development of the linac tune for uranium ions starts with the precalculated setting of all beam optics devices and rf cavities for the entire linac. A model-based linac setting is not sufficient to achieve no-beam-loss tuning. Low beam losses along the linac are critical for the operation of heavy ions at high power. To minimize losses, we have developed physics applications to fine-tune the linac from the FE to the target and expedite the linac tuning process [14,15]. The rf cavities' phases and amplitudes for any given ion species and its energy are calculated using a model-based instant phase setting (IPS) procedure as described in Ref. [16]. The IPS relies on alignment survey data, the phase offset, field amplitude calibration of each resonator, and the beam position monitors (BPMs) phase relative to the master clock. Such calibration is performed by the phase scan procedure of each cavity and can take up to 24 h for the 324 superconducting resonators. Our experience shows that this calibration is exceedingly stable and remains unchanged for many months. We applied the IPS procedure to accelerate $^{238}\text{U}^{35+}$ to 17.0 MeV/u to the location of the stripper. Nearly all superconducting cavities in the pre-stripper section were operated at 100% of their designed accelerating gradients. At the LS2 and LS3, the phasing of the resonators was also performed using the IPS application for the central charge state $^{238}\text{U}^{75+}$. The 3D beam envelope code flame imports the IPS setting of the rf cavities and generates the optimal setting of all linac devices as a file. The "Setting Manager" application [17] in the accelerator controls network imports the flame-generated file and applies it to the linac devices.

To complete beam tuning in the linac, we applied beam steering corrections and provided matching in the transverse phase space in seven linac sections. In these sections, the quadrupole settings were adjusted with respect to the flame calculations and based on beam profile measurements and evaluation of the beam root mean square (rms) Courant-Snyder (CS) parameters [18]. The latter were calculated using either (a) a quadrupole scan and profile measurements or (b) profile measurements in multiple locations. We use the orbit response matrix (ORM) method [18,3] based on the flame model for the beam steering correction.

The evaluation of the beam rms CS parameters in the transverse phase space is required upstream of the following linac segments: (i) LS1, to match the beam into the quasiperiodic solenoidal focusing channel; (ii) stripper, to obtain the required beam rms size on the stripper; (iii) FS1, to match into the 180° achromatic bend; (iv) LS2, to match the beam into the quasiperiodic solenoidal focusing channel; (v) FS2, to match into the 180° achromatic bend; (vi) LS3, to match into the focusing channel; (vii) BDS, to

match into the 70° achromatic bend and form the required beam spot on the target.

The deviation of the beam CS parameters from those calculated by the envelope code flame is caused by multiple factors. Examples are as follows: (i) The uncontrollable 4D distribution caused by the beam exiting the ECR magnetic field; (ii) the dynamics of a multicomponent ion beam with an unknown degree of beam neutralization in the LEBT; (iii) the contribution of realistic 3D field distributions in all focusing devices (flame uses a hard-edge equivalent model); (iv) the hysteresis of magnetic fields.

IV. CHARGE STRIPPING

To overcome the technical limitations associated with stripping high-intensity heavy ion beams with thin foils, FRIB developed and commissioned a liquid lithium stripper [19]. The charge stripper uses a molten liquid lithium film with a $\sim 10\text{--}20\ \mu\text{m}$ thickness, flowing at $\sim 60\ \text{m/s}$ in the vacuum environment. The 17.0 MeV/u uranium beam was focused into a small spot with $\sim 0.4\ \text{mm}$ rms radius on the lithium film, and its position was adjusted to minimize the film's nonuniformity negatively impacting the beam energy spread. Based on the previous measurements [19], the film's nonuniformity under the beam spot was less than 6%. The beam energy loss in the stripper was 500 keV/u, corresponding to the $1.08\ \text{mg/cm}^2$ film thickness. The measured and simulated charge state distributions are shown in Fig. 3. The simulations were performed with the ETACHA4-GUI code [20] updated into the framework of the $\text{LISE}_{\text{cute}}^{++}$ package [21]. Unfortunately, the lithium film thickness currently cannot produce an equilibrium charge distribution for ion species heavier than argon. For efficient use of the available accelerating voltage, the central charge state for the uranium beam should be $78+$. Ongoing R&D work seeks to double the lithium film thickness [22].

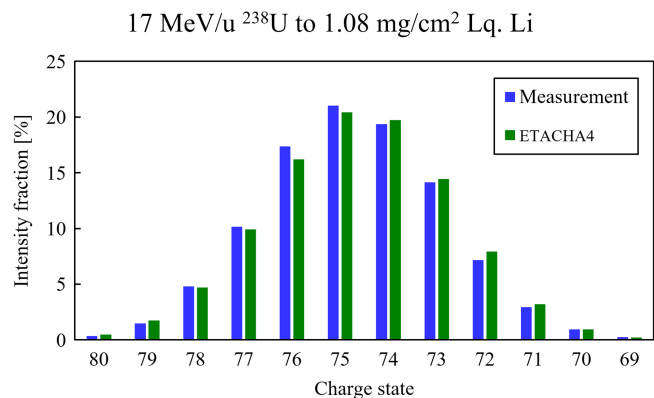


FIG. 3. Measured and simulated charge state distributions of uranium beam with the incident energy of 17.00 MeV/u after liquid lithium stripper.

V. 3-Q URANIUM TUNING IN THE LINAC

FRIB linac was designed to simultaneously accelerate multiple charge-state heavy ion beams to deliver high-power beams to the target [4]. The theory of multiple-charge-state beams in a superconducting linac was reported earlier [23]. Several years ago, a three-charge-state xenon beam was accelerated in the FRIB linac [24] that presents simulated and measured beam parameters in transverse and longitudinal phase space. Since then, the quality of multiple-charge-state tuning has been significantly improved. Therefore, on-target 10.4 kW beam power was achieved by accepting three charge states $3-q$ of $^{238}\text{U}^{74+,75+,76+}$ after the stripper, resulting in 58% stripping efficiency, and accelerating them to 177 MeV/u. Avoiding effective emittance growth and eventually maintaining low uncontrolled beam losses were achieved by carefully matching the rms CS parameters of the $3-q$ beam in the 6D phase space and minimizing coherent oscillations in the transverse and longitudinal phase space. The recombination of the $3-q$ beam position in the transverse phase space after the bending segments, FS1, FS2, and BDS, was achieved by precise tuning of the achromatic bends and correction of the chromatic aberrations due to the charge spread, $\Delta q/q = \pm 1.33\%$. The achromat tuning includes three main steps applied to the dispersive plane: (i) The trajectory of the central charge state $75+$ was tuned to the center of two pairs of quadrupoles between the bending magnets using two steering correctors; one of them is the bending magnet itself; (ii) the strengths of the quadrupoles affecting the dispersion were adjusted simultaneously to achieve the same transverse positions of charge states $74+$ and $76+$ at the exit of the achromatic bend; (iii) adjustment of a pair of sextupoles to steer the position of both charge states $74+$ and $76+$ to the center of the downstream beamline.

Figure 4 shows the adjustment of quadrupoles and sextupoles relative to the FLAME predictions Q_0 and S_0 to achieve the required position of the $3-q$ beam after the achromatic bend. This procedure was applied in all three bending segments, FS1, FS2, and BDS, to minimize the effective transverse emittance growth. Using this procedure, the experimentally found optimized settings of the quadrupoles in the achromatic bends were consistent within 3% of the FLAME optimization. The slight discrepancy is likely due to the deviation of the 3D field maps from those used in FLAME's hard-edge equivalent model. The beam steering correction in the straight segments LS2 and LS3 was performed only for the central charge state $75+$. This was sufficient to maintain the transverse positions of charge states $74+$ and $76+$ within ± 1.6 mm with respect to the central charge state as shown in Fig. 5. Phasing of cavities in LS2 and LS3 was performed for the central charge state $75+$ using the IPS application. At the entrance of the LS2, the bunch centers of each charge state $74+$, $75+$, and $76+$ in the longitudinal phase space were nearly identical thanks to the rebuncher focusing. Envelope

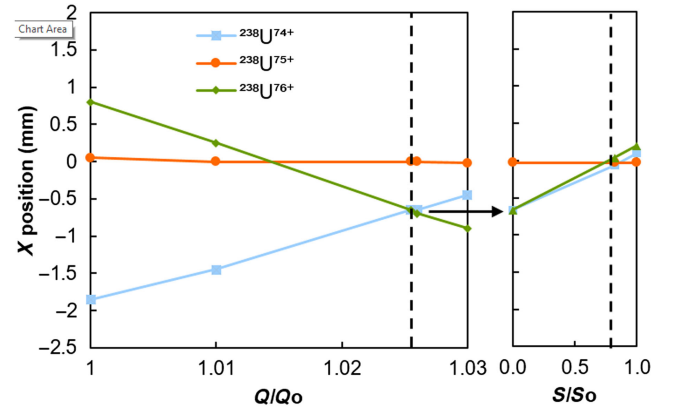


FIG. 4. Horizontal positions of charge state $74+$, $75+$, and $76+$ after the achromatic bend as a function of quadrupoles' (left) and sextupoles' (right) strength in the dispersive plane. The vertical dash line shows the optimal setting of the quadrupoles and sextupoles.

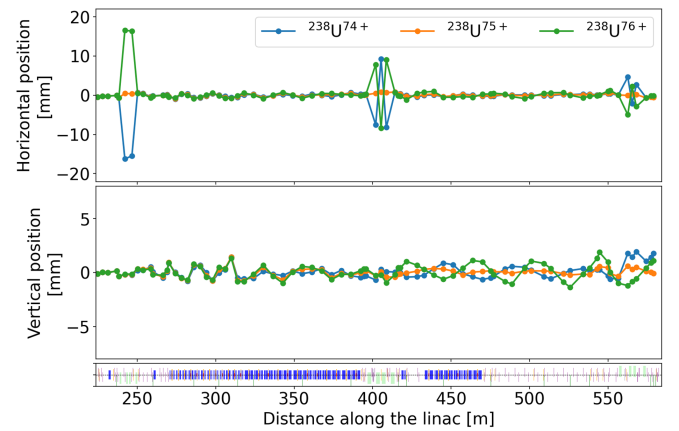


FIG. 5. Measured transverse beam position of each charge state beam along the poststripper linac. Note the scale in the dispersive plane is larger.

mapping [16] performed for each charge state separately confirms the validity of this approach, as shown in Fig. 6.

To match multiple charge state beams to the target, we evaluated the rms CS parameters for each charge state from

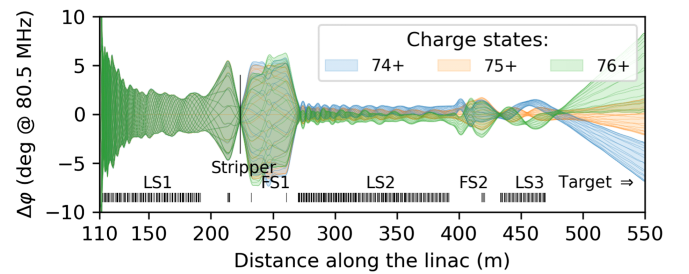


FIG. 6. Longitudinal mapping of individual charge states $74+$, $75+$, and $76+$ for a ^{238}U beam in the entire linac. $\Delta\phi$ is the difference in the phase signals induced in the BPMs.

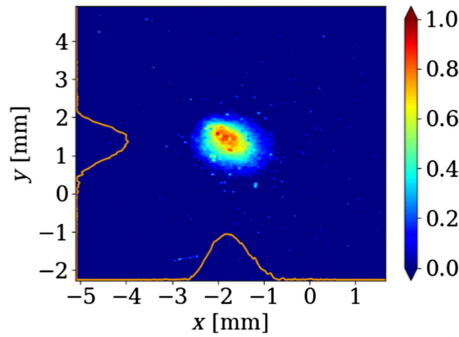


FIG. 7. Thermal image of 300 W uranium beam on the static target.

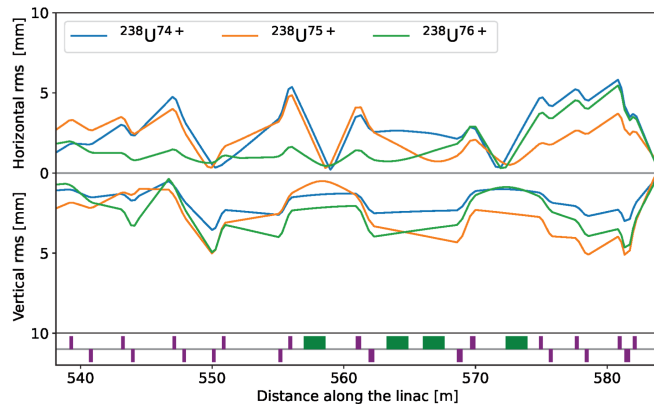


FIG. 8. rms envelopes of three charge states of ^{238}U beam matched simultaneously into the target.

the profile measurements and adjusted fields in eight quadrupoles upstream of the BDS to obtain the beam waist on the target position with the 0.35-mm rms radius. The 300-W beam image on the static target is shown in Fig. 7. The matched beam envelopes for each charge state of the uranium beam are shown in Fig. 8. Using only the central charge state to match the 3-q beam is insufficient to avoid beam losses in the BDS.

The thermal image of the 10.4-kW 3-q ^{238}U beam on the rotating carbon target is shown in Fig. 9. The target was rotated with an angular speed of 500 rpm. The temperature of the target under the beam trace was $\sim 1010^\circ\text{C}$. The beam tuning and accelerator setup are usually performed with a low average power pulsed beam. After completing the tuning, the uranium beam power was ramped up to 10.4 kW.

We observed a temperature increase of up to 0.3 K in the beam pipe in the LS2 cryomodules due to the beam losses in several locations. Based on the calibration of thermal sensors on the cryogenic beam pipes, these losses correspond to ~ 0.5 W. After the passage of the stripper, ion beams experience an energy spread increase due to straggling in the stripper and liquid lithium film nonuniformity. A small fraction of ions is outside the longitudinal

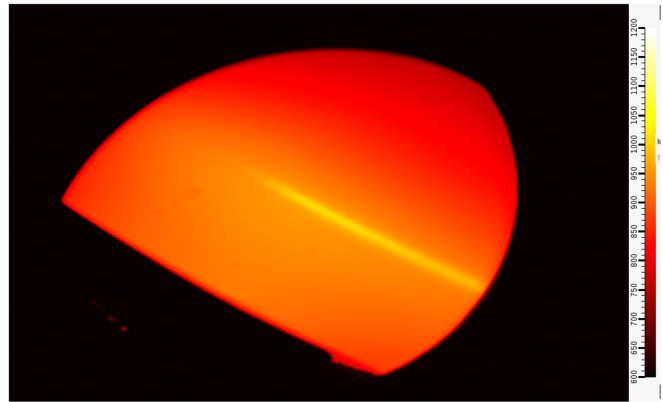


FIG. 9. Thermal image of the 177 MeV/u three-charge-state ^{238}U beam on the target. The target rotated counterclockwise at 500 rpm resulting in the strip seen in the image.

acceptance of the poststripper linac section, which gets lost in the LS2. The simulations show that the unaccepted particles are lost near the solenoid in the third cryomodule in LS2, where we measure the highest increase in the beam pipe temperature. The temperature increase data in the third cryomodule for many ion species from ^{18}O to ^{238}U is illustrated in Fig. 10 as a function of the mass number. Each ion species is delivered to the target at the same 10 kW beam power. The uranium beam experiences the highest energy loss in the stripper and the most potent energy straggle compared to any other ions, which results in the highest temperature increase for the beam pipe. To maintain acceptable beam losses in LS2 as beam power ramps up, we plan to increase the longitudinal acceptance by linearizing the 161-MHz multigap rebuncher [25] (position 7 in Fig. 1) voltage over an extended phase range by using the second harmonic rf cavity [15]. The second harmonic cavity, in

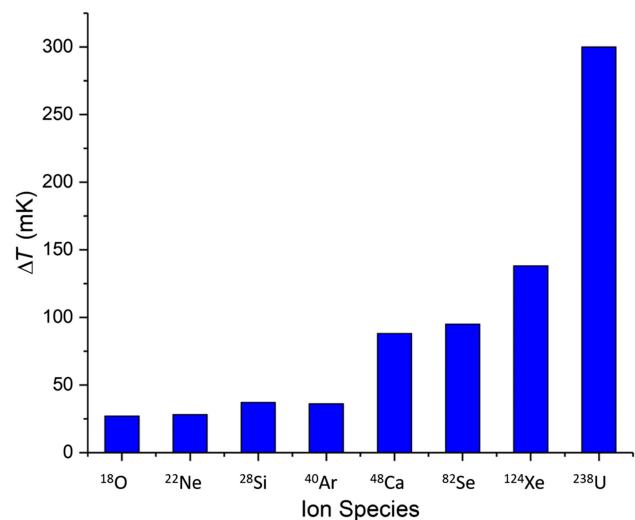


FIG. 10. The highest temperature increase of the beam pipe in the third cryomodule of the LS2 as a function of ion species (mass number).

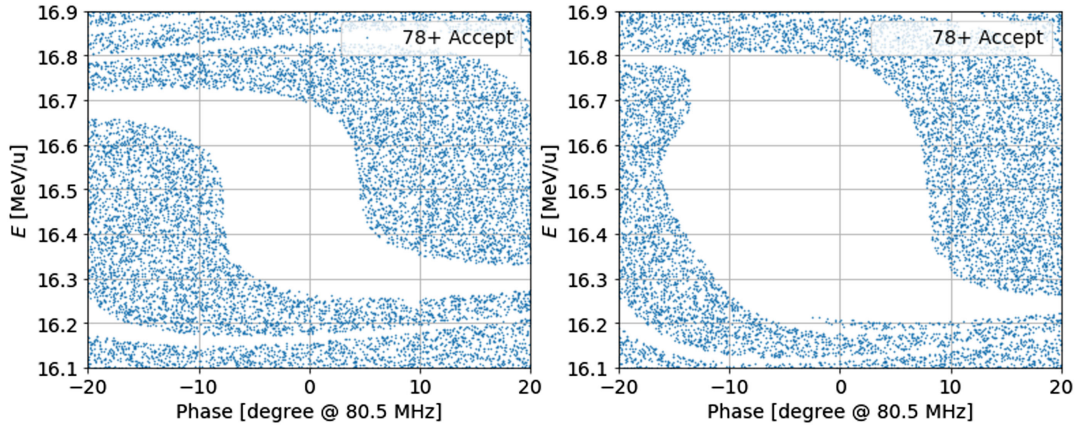


FIG. 11. Simulated longitudinal phase-space acceptance of the linac section downstream of the stripper for three charge states of $^{238}\text{U}^{78+}$ without (left) and with (right) the second-harmonic cavity.

combination with a 161-MHz buncher in both locations shown in Fig. 1, significantly increases longitudinal acceptance as illustrated in Fig. 11 in the example for $^{238}\text{U}^{78+}$ beam.

During the operation, we also noticed occasional sudden changes in the lithium film thickness for 1–2 min, which resulted in $\sim 0.26\%$ beam energy change after the stripper. These events result in a beam loss increase in the FS2 and BDS. The uncontrolled beam losses in the linac are below 10^{-4} , but they can be monitored thanks to the high sensitivity of beam loss monitors (ion chambers and neutron detectors). After the completion of the uranium beam operation, a radiation survey was performed in the accelerator tunnel, which showed the residual activation was well below 0.1 mR/h in all areas.

VI. OBSERVATION OF NEW ISOTOPES

The new high-power primary beam of ^{238}U nuclei with energy 177 MeV/u was focused on a rotating 2.1-mm thick carbon target wheel ($\rho = 1.89 \text{ g/cm}^3$) at the start of the Advanced Rare Isotope Separator (ARIS) [26,2]. The ion optics of ARIS [26] were used in momentum-compression mode to separate and identify the nuclides produced from the fission of the ^{238}U beam in the target. The C-bend section of ARIS served as two high-acceptance stages enabling effective particle separation in the middle- Z region.

The particles of interest were stopped in a silicon PIN diode telescope consisting of seven silicon detectors located at the final focal plane of ARIS. The event-by-event identification of each heavy ion in this study involved the combined measurement of the magnetic rigidity ($B\rho$), time of flight (ToF), energy loss (ΔE), and total kinetic energy (TKE) as described in the appendix of Ref. [27] and more recently in the first FRIB new isotope search [28]. A germanium γ -ray detector was placed close to the Si telescope to provide an independent particle identification

verification by observing the known ^{94}Br isomer decay ($T_{1/2} = 0.53 \mu\text{s}$) [29].

To search for new neutron-rich isotopes with $30 \leq Z \leq 35$, the separator was tuned to optimize the transmission of the $^{93}\text{As}^{33+}$ ion based on calculations with the $\text{LISE}_{\text{cute}}^{++}$ code [21,30]. With the ARIS separator momentum acceptance set to $\Delta p/p = 2.3\%$ and using an Al wedge with a thickness of 1 mm, over the course of 6-h runs, three never-before observed isotopes were identified: ^{88}Ga (two events), ^{93}As (seven events), and ^{96}Se (two

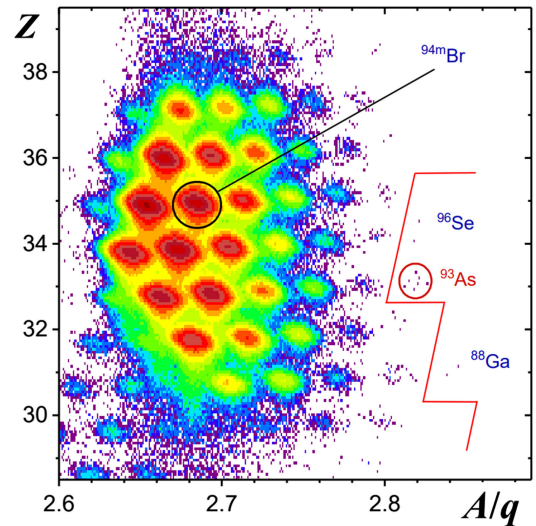


FIG. 12. The particle identification (PID) plot with the atomic number, Z , identification for the fully stripped ions as a function of mass to charge, A/q . The mass-to-charge ratio, A/q , was constructed from flight time through the separator, and the magnetic rigidity measured ion-by-ion for runs set on ^{93}As production. This PID plot demonstrates the quality of the mass and elemental separation. The solid red line indicates the limit of previously observed nuclei, and location of ^{93}As is marked. A γ -ray spectrum observed in coincidence with the labeled ^{94}Br isotopes was used to confirm its identification.

events). The particle identification matrix of fully striped reaction products observed in these runs is shown in Fig. 12. Additionally, unambiguous identification of fragments in the middle-Z region was achieved, produced during a brief run with the separator tuned to the $^{152}\text{Cs}^{55+}$ ion.

After we submitted our manuscript on February 13, 2024, we learned that the paper [31], in which the authors observed two new isotopes, ^{88}Ga and ^{93}As , had been accepted for publication.

VII. SUMMARY

The accelerator facility at FRIB produced the highest-power accelerated cw uranium beam ever seen, leading to the separation and identification of three previously unknown isotopes. This achievement was possible thanks to the successful operation of FRIB, including a new superconducting linear accelerator composed of 324 resonators in 46 cryomodels, a newly developed liquid lithium stripper, and other novel technologies such as uranium production in the ECR, the unique heavy-ion RFQ, the high-power target, and beam dump. New techniques were developed to set up the simultaneous acceleration of three charge states of uranium after stripping with liquid lithium film and were successfully applied to achieve the record-high power of uranium. The experience gained with uranium operation was invaluable; in order to continue our push to higher uranium intensities, the following improvements will be required: (i) Develop robust and fast beam profile measurement tools to expedite accelerator setup time, especially for multiple-charge-state beams; (ii) develop and implement the second harmonic cavity to increase the longitudinal acceptance of the poststripper linac, as previously proposed [12]; (iii) continue the development of a feedback loop to stabilize the beam energy after the stripper [12].

ACKNOWLEDGMENTS

The authors are grateful to the entire FRIB team for supporting the facility operation during the experiments with the uranium beam and the production of new isotopes. This material is based upon work supported by the U.S. Department of Energy, Office of Science, Office of Nuclear Physics, and used resources of the FRIB Operations, which is a DOE Office of Science User Facility under Award No. DE-SC0023633. This work was also supported by the U.S. National Science Foundation under Grant No. PHY-23-10078. D. S. A. and J. H. acknowledge the support from the IBS Grants No. IBS-R031-D1 and No. IBS-R031-Y2.

[1] J. Wei *et al.*, Accelerator commissioning and rare isotope identification at the Facility for Rare Isotope Beams, *Mod. Phys. Lett. A* **37**, 2230006 (2022).

- [2] M. Portillo *et al.*, Commissioning of the Advanced Rare Isotope Separator ARIS at FRIB, *Nucl. Instrum. Methods Phys. Res., Sect. B* **540**, 151 (2023).
- [3] P. N. Ostroumov, M. Hausmann, K. Fukushima, T. Maruta, A. S. Plastun, M. Portillo, J. Wei, T. Zhang, and Q. Zhao, Heavy ion beam physics at Facility for Rare Isotope Beams, *J. Instrum.* **15**, P12034 (2020).
- [4] Q. Zhao, A. Facco, F. Marti, E. Pozdeyev, M. J. Syphers, J. Wei, X. Wu, Y. Yamazaki, and Y. Zhang, FRIB accelerator beam dynamics design and challenges, in *Proceedings of HB2012, Beijing, China* (JACoW, Geneva, Switzerland, 2012), p. 404, <https://accelconf.web.cern.ch/HB2012/>.
- [5] J. Wei *et al.*, FRIB beam power ramp-up: Status and plans, in *Proceedings of 68th Advanced Beam Dynamics Workshop High-Intensity High-Brightness Hadron Beams HB2023, CERN, Geneva, Switzerland* (JACoW, Geneva, Switzerland, 2023), p. 351, <https://accelconf.web.cern.ch/hb2023/papers/thc1i2.pdf>.
- [6] J. F. Ahearn *et al.*, Opportunities with a rare-isotope facility in the United States Rare-Isotope Science Assessment Committee (RISAC), Report of the National Research Council of the National Academies, Prepublication Report December 8, 2006, <https://nap.nationalacademies.org/catalog/11796/scientific-opportunities-with-a-rare-isotope-facility-in-the-united-states>.
- [7] J. Symons *et al.*, Report to NSAC of the rare-isotope Beam Task Force, 2007, <https://www.jinaweb.org/sites/default/files/inline-files/2007%20-%20report%20to%20NSAC.pdf>.
- [8] K. Yamada, Upgrade and current status of high-frequency systems for RIKEN ring cyclotron, in *Proceedings of 23rd International Conference on Cyclotrons Applications Cyclotrons 2022, Beijing, China* (JACoW, Geneva, Switzerland, 2022), MOAI02, p. 6, <https://accelconf.web.cern.ch/cyclotrons2022/papers/moai02.pdf>.
- [9] RIBF Users' Information, <https://www.nishina.riken.jp/RIBF/accelerator/tecinfo.html>.
- [10] H. Ren *et al.*, Development and status of the FRIB 28 GHz SC ECRIS, *J. Phys. Conf. Ser.* **2244**, 012008 (2022).
- [11] L. T. Sun, D. Leitner, G. Machicoane, E. Pozdeyev, V. Smirnov, S. B. Vorozhtsov, D. Winklehner, and Q. Zhao, Low energy beam transport for facility for rare isotope beams driver linear particle accelerator, *Rev. Sci. Instrum.* **83**, 02B705 (2012).
- [12] Z. He, Y. Zhang, J. Wei, Z. Liu, and R. M. Talman, Linear envelope model for multi-charge state linac, *Phys. Rev. ST Accel. Beams* **17**, 034001 (2014).
- [13] K. Hwang, T. Maruta, A. Plastun, K. Fukushima, T. Zhang, Q. Zhao, P. Ostroumov, and Y. Hao, Prior-mean-assisted Bayesian optimization application on FRIB front-end tuning, [arXiv:2211.06400](https://arxiv.org/abs/2211.06400).
- [14] P. N. Ostroumov, K. Fukushima, T. Maruta, A. Plastun, J. Wei, T. Zhang, K. Hwang, and Q. Zhao, Accelerator and beam physics challenges in support of FRIB experiments, in *Proceedings of the 14th International Particle Accelerator Conference, IPAC-2023, Venice, Italy* (JACoW, Geneva, Switzerland, 2023), <https://accelconf.web.cern.ch/ipac2023/pdf/TUPA180.pdf>.
- [15] P. N. Ostroumov, K. Fukushima, A. Gonzalez, K. Hwang, T. Kanemura, T. Maruta, A. Plastun, J. Wei, T. Zhang, and Q. Zhao, FRIB from commissioning to operation, in

- Proceedings of the 68th Adv. Beam Dyn. Workshop High-Intensity High-Brightness Hadron Beams, HB2023, Geneva, Switzerland* (CERN, Switzerland, 2023), p. 9, <https://accelconf.web.cern.ch/hb2023/papers/moali2.pdf>.
- [16] A. S. Plastun and P. N. Ostroumov, Instant phase setting in a large superconducting linac, in *Proceedings of 5th North American Particle Accelerator Conference, Albuquerque, NM* (JACoW, Geneva, Switzerland, 2022), p. 885, <https://accelconf.web.cern.ch/napac2022/papers/thzd1.pdf>.
- [17] T. Zhang, K. Fukushima, T. Maruta, P. Ostroumov, A. Plastun, and Q. Zhao, Manage the physics settings on a modern accelerator, in *Proceedings of the 18th International Conference on Accelerator and Large Experimental Physics Control Systems, ICALEPCS2021, Shanghai, China* (JACoW, Geneva, Switzerland, 2021), p. 569, <https://accelconf.web.cern.ch/icalcps2021/papers/web104.pdf>.
- [18] P. N. Ostroumov *et al.*, Beam commissioning in the first superconducting segment of the Facility for Rare Isotope Beams, *Phys. Rev. Accel. Beams* **22**, 080101 (2019).
- [19] T. Kanemura, M. LaVere, R. Madendorp, F. Marti, T. Maruta, Y. Momozaki, P. N. Ostroumov, A. S. Plastun, J. Wei, and Q. Zhao, Experimental demonstration of the thin-film liquid-metal jet as a charge stripper, *Phys. Rev. Lett.* **128**, 212301 (2022).
- [20] E. Lamour, P. D. Fainstein, M. Galassi, C. Prigent, C. A. Ramirez, R. D. Rivarola, J.-P. Rozet, M. Trassinelli, and D. Vernhet, Extension of charge-state-distribution calculations for ion-solid collisions towards low velocities and many-electron ions, *Phys. Rev. A* **92**, 042703 (2015).
- [21] O. B. Tarasov, D. Bazin, M. Hausmann, M. P. Kuchera, P. N. Ostroumov, M. Portillo, B. M. Sherrill, K. V. Tarasova, and T. Zhang, LISE⁺⁺_{cute}, the latest generation of the LISE package, to simulate rare isotope production with fragment-separators, *Nucl. Instrum. Methods Phys. Res., Sect. B* **541**, 4 (2023).
- [22] T. Kanemura *et al.*, Operational performance with FRIB liquid lithium and carbon charge strippers, in *Proceedings of 68th Advanced Beam Dynamics Workshop High-Intensity High-Brightness Hadron Beams HB2023, CERN, Geneva, Switzerland* (JACoW, Geneva, Switzerland, 2023), paper WEC2I2, to be published, pre-press proceedings, https://hb2023.vrws.de/talks/wec2i2_talk.pdf.
- [23] P. N. Ostroumov and K. W. Shepard, Multiple-Charge Beam Dynamics in an Ion Linac, *Phys. Rev. ST Accel. Beams* **3**, 030101 (2000).
- [24] P. N. Ostroumov, K. Fukushima, T. Maruta, A. S. Plastun, J. Wei, T. Zhang, and Q. Zhao, First simultaneous acceleration of multiple charge states of heavy ion beams in a large-scale superconducting linear accelerator, *Phys. Rev. Lett.* **126**, 114801 (2021).
- [25] P. N. Ostroumov, A. S. Plastun, N. Bultman, D. Morris, X. Rao, Q. Zhao, and S. Zhao, Efficient continuous wave accelerating structure for ion beams, *Phys. Rev. Accel. Beams* **23**, 042002 (2020).
- [26] M. Hausmann *et al.*, Design of the Advanced Rare Isotope Separator ARIS at FRIB, *Nucl. Instrum. Methods Phys. Res., Sect. B* **317**, 349 (2013).
- [27] O. B. Tarasov *et al.*, Production of very neutron-rich nuclei with a ⁷⁶Ge beam, *Phys. Rev. C* **80**, 034609 (2009).
- [28] O. B. Tarasov, A. Gade, K. Fukushima, M. Hausmann, E. Kwan *et al.*, Observation of new isotopes in the fragmentation of ¹⁹⁸Pt at FRIB, *Phys. Rev. Lett.* **132**, 072501 (2024).
- [29] D. Kameda *et al.*, Observation of new microsecond isomers among fission products from in-flight fission of 345 MeV/nucleon ²³⁸U, *Phys. Rev. C* **86**, 054319 (2012).
- [30] O. B. Tarasov and D. Bazin, LISE⁺⁺: Radioactive beam production with in-flight separators, *Nucl. Instrum. Methods Phys. Res., Sect. B* **266**, 4657 (2008).
- [31] Y. Shimizu, T. Kubo, T. Sumikama, N. Fukuda, H. Takeda *et al.*, Production of new neutron-rich isotopes around the N = 60 isotones ⁹²Ge and ⁹³As by in-flight fission of a 345 MeV/nucleon ²³⁸U beam, *Phys. Rev. C* **109**, 044313 (2024).